Carbohydrate Polymers 92 (2013) 380–387

Contents lists available at SciVerse ScienceDirect

Carbohydrate Polymers

journal homepage: www.elsevier.com/locate/carbpol

Synthesis and characterization of multi-amino-functionalized cellulose for arsenic adsorption

Xiaolin Yu[a], Shengrui Tong[a,*], Maofa Ge[a,**], Lingyan Wu[a], Junchao Zuo[a], Changyan Cao[b], Weiguo Song[b]

[a] Beijing National Laboratory for Molecular Sciences (BNLMS), State Key Laboratory for Structural Chemistry of Unstable and Stable Species, Institute of Chemistry, Chinese Academy of Sciences, Beijing 100190, PR China
[b] Laboratory for Molecular Nanostructures and Nanotechnology, Institute of Chemistry, Chinese Academy of Sciences, Beijing 100190, PR China

ARTICLE INFO

Article history:
Received 5 July 2012
Received in revised form 1 August 2012
Accepted 24 September 2012
Available online 2 October 2012

Keywords:
Adsorbent
Adsorption
Arsenic
Isotherm model

ABSTRACT

A multi-amino adsorbent for arsenic adsorption was reported in this paper. Glycidyl methacrylate (GMA) was first grafted onto the surface of cotton cellulose using ceric ammonium nitrate (CAN) as the initiator, and then the introduced epoxy groups reacted with tetraethylenepentamine (TEPA) to obtain a multi-amino adsorbent. The adsorbent was characterized by FTIR, elemental analysis, ^{13}C NMR and SEM. Then, the adsorption of arsenic for this adsorbent was investigated. The results showed that the GMA and TEPA were successfully grafted onto the surface of cellulose, and the modification improved the arsenic adsorption performances. Kinetic study suggested that the chemisorptions were the rate-limiting step. Among the three adsorption isotherm models used, Langmuir model fitted the experimental data best. The adsorption capacities of arsenic were less affected by coexisting ions. The adsorbent could be effectively regenerated for four cycles with 0.1 mol/L NaOH solution.

© 2012 Elsevier Ltd. All rights reserved.

1. Introduction

Arsenic is one of the most toxic and ubiquitous element in the environment (Chandra et al., 2010; Zhao, Jia, Xu, & Zhao, 2011). In the aquatic environment the most common species of arsenic exist as the oxidation states of inorganic arsenite As(III) and arsenate As(V) (Munoz, Gonzalo, & Valiente, 2002), which plays an important role in the arsenic properties, such as toxicity, surface charge and mobilization. Arsenic is classified as a carcinogen by United State Environmental Protection Agency (USEPA) (Dhoble, Lunge, Bhole, & Rayalu, 2011). The chronic exposure to arsenic can lead to serious adverse impacts on human health, such as skin, lung, bladder and kidney cancers (An, Liang, & Zhao, 2011; Wu, Li, Webley, & Zhao, 2012). According to the World Health Organization (WHO) criteria, the concentration of arsenic in public water supplies should be no more than 10 ppb (Chandra et al., 2010; Tian, Wu, Lin, Huang, P., & Huang, Y., 2011).

Various treatment methods such as oxidation (Martin, O'Donnell, Martin, & Alldredge, 2007), coagulation (Moreno-Casillas et al., 2007), ion exchange (Anirudhan & Unnithan, 2007), chemical precipitation (Mercer & Tobiason, 2008), membrane separation (Iqbal, Kim, Yang, Baek, & Yang, 2007) and adsorption (Maji, Pal, Pal, & Adak, 2007) have been used to remove arsenic from the aqueous solution. Amongst all the treatment processes mentioned, adsorption is recognized as an effective approach due to the low cost, high concentration efficiency and environmental friendly behavior (Gu, Fang, & Deng, 2005; O'Connell, Birkinshaw, & O'Dwyer, 2008).

Cellulose, the most widely available and renewable biopolymer in nature, is a very promising raw material available at low cost for the preparation of various functional materials. Due to the present of hydroxyl groups, cellulose is considered to be an excellent material for surface modification (Habibi, Lucia, & Rojas, 2010). Among the chemical modification methods, grafting copolymerization offers an attractive and versatile technique of imparting a variety of functional group to cellulose in order to improve the adsorption capacities of cellulose (Roy, Semsarilar, Guthrie, & Perrier, 2009). Glycidyl methacrylate (GMA) monomer has dual functionality, methacrylic and epoxy groups, which can be used as the precursor monomer. After grafting GMA onto cellulose, reactive epoxy groups can be introduced into cellulose, and further react with other functional groups capable of adsorbing anion pollutants in aqueous solution. The amine functional groups, such as $-NH_2$, $-NRH$ and NR_1R_2, can be protonated to form $-NH_3^+$, $-NRH_2^+$ and $-NR_1R_2H^+$ in aqueous solution, which have the ability to adsorb the anion pollutants through electrostatic interaction. Various cellulosic materials modified with polyamine have been used for anion removal (Cao et al., 2011; Gurgel, de Melo, de Lena, & Gil, 2009; Xu et al., 2011; Xu, Gao, Yue, Zhong, & Zhan,

* Corresponding author. Tel.: +86 10 62558682; fax: +86 10 62559373.
** Corresponding author. Tel.: +86 10 62554518; fax: +86 10 62559373.
E-mail addresses: tongsr@iccas.ac.cn (S. Tong), gemaofa@iccas.ac.cn (M. Ge).

0144-8617/$ – see front matter © 2012 Elsevier Ltd. All rights reserved.
http://dx.doi.org/10.1016/j.carbpol.2012.09.050

2010). Tian, Wu, Liu, et al. (2011) prepared a tertiary amine-based cellulosic adsorbent with N,N-Dimethylaminoethyl methacrylate for the removal of arsenic and found that the adsorption capacity of arsenic could reach 8.96 mg/g for As(III) and 27.93 mg/g for As(V), respectively. Anirudhan and Unnithan (2007) synthesized an amino-functionalized anion cellulosic adsorbent with dimethylamine to remove arsenic from aqueous solution and the As(V) adsorption capacity was 13.57 mg/g. To our knowledge, however, there are no reports about multi-amino-functionalized cellulose for the removal of arsenic, including primary amine, secondary amine and tertiary amine.

In the present study, we prepared a multi-amino adsorbent by grafting GMA onto cotton using ceric ammonium nitrate (CAN) as the initiator, and further introducing multi-amino groups via ring-opening reaction with tetraethylenepentamine (TEPA) on the surface of graft copolymers. The modified cellulose was characterized by FTIR, elemental analysis, ^{13}C NMR and SEM and then was used for the removal of arsenic from aqueous solution. The effects of contact time, pH, initial adsorption concentration, coexisting ions and the regeneration performance were investigated.

2. Materials and methods

2.1. Materials

Medical absorbent cotton cellulose was obtained from Jiaozuo league Hygiene Group (China). Ceric ammonium nitrate (CAN), tetraethylenepentamine (TEPA), dimethylformamide (DMF) were purchased from Sinopharm Chemical Reagent Co., Ltd. Glycidyl methacrylate (96%, GMA), sodium arsenite ($NaAsO_2$) and sodium arsenate dibasic ($Na_2HAsO_4{\cdot}7H_2O$) were obtained from J&K Scientific Ltd. All the solvents and reagents were used without further purification.

2.2. Synthesis of cellulose-g-GMA and cellulose-g-GMA-b-TEPA

Cotton cellulose (10 g) was first treated with 100 mL of aqueous NaOH solution (20%, w/v) at 25 °C for 6 h in order to obtain alkali cellulose, and then alkali cellulose was washed with distilled water up to pH 7. Finally, the alkali cellulose was dried in vacuum at 60 °C.

The PGMA chains were grafted onto the alkali cellulose surface by the ceric ion (Ce^{4+}) initiated polymerization (O'Connell, Birkinshaw, & O'Dwyer, 2006; Zhou, Jin, Zhu, & Akama, 2011). Alkali cellulose (3 g) was dispersed in 200 mL 0.1 mol/L CAN aqueous solution, and then 0.4 mL nitric acid was added. The mixtures were first carried out at 30 °C for 15 min under the nitrogen atmosphere, then GMA (10 mL) was added, and the mixtures were reacted at 30 °C for 3 h. The PGMA grafted alkali cellulose (cellulose-g-GMA) was soxhlet extracted with acetone/methanol (1:1) for 24 h to remove all the GMA homopolymer, and then dried in vacuum at 60 °C. The graft percentage was calculated by the percent increase in mass as follows:

$$G\% = \frac{m_g - m_0}{m_0} \times 100 \quad (1)$$

where m_g (g) and m_0 (g) are the mass of the grafted and the initial celluloses, respectively.

Cellulose-g-GMA (5 g) was dispersed in 250 mL DMF solution, and then 25 mL TEPA was added. The reaction was carried out at 100 °C for 12 h. The synthetic route of cellulose-g-GMA-b-TEPA is shown in Scheme 1. The amine-functionalized products (cellulose-g-GMA-b-TEPA) were filtered, washed with distilled water and acetone, and then dried in vacuum at 60 °C. The mass gain percent (Mgp) was calculated according to

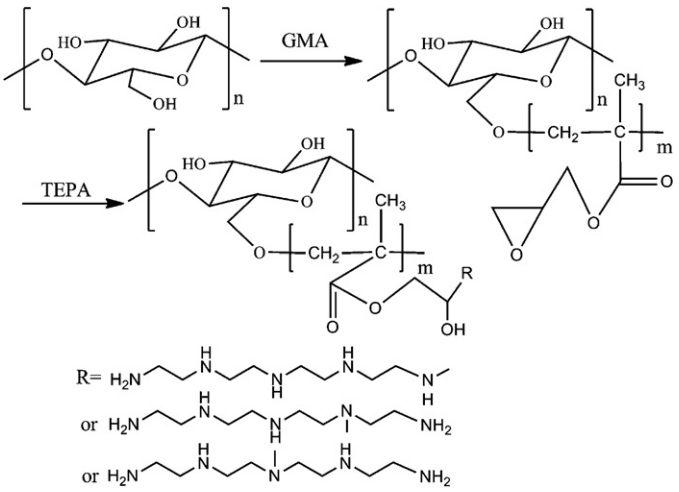

Scheme 1. Synthetic route for the cellulose-g-GMA-b-TEPA.

$$\text{Mgp}\% = \frac{m_a - m_g}{m_g} \times 100 \quad (2)$$

where m_a (g) and m_g (g) are the mass of the aminated and the grafted celluloses, respectively.

2.3. Characterization of materials

The content of epoxy groups in cellulose-g-GMA was determined by the pyridine–HCl titration method (Anirudhan & Senan, 2011). 0.5 g–1 g cellulose-g-GMA was refluxed with 20 mL pyridine–HCl mixture (0.32 mL HCl and 19.68 mL pyridine) at 128 °C for 20 min. After cooling the solution, condenser tube was washed with 15 mL acetone. The above solution was back-titrated with 0.1 mol/L NaOH solution using phenolphthalein solution as indicator until the solution turned from colorless to the pale pink. The epoxy group content of cellulose-g-GMA (Egc, mmol/g) was calculated by using the following equation:

$$\text{Egc} = \frac{(V_0 - V_1)C_{\text{NaOH}}}{m} \quad (3)$$

where V_0 (mL) and V_1 (mL) are the consumed volume of NaOH in titrating blank and sample, respectively, C_{NaOH} (mol/L) is the amount of known NaOH molarity, m (g) is the weight of the analyzed sample.

The content of nitrogen in cellulose-g-GMA-b-TEPA was analyzed by using flash EA 1112 elemental analyzer. A Thermo Nicolet 6700 Fourier transform infrared spectroscopy (FTIR) were used to verify the presence of functional groups in the adsorbent. The solid-state CP/MAS ^{13}C NMR spectra of the sample were obtained on a Bruker Avance III 400 spectrometer. The morphology of the samples was observed by Hitachi S-4300 scanning electron microscope (SEM) operating at 15 kV. The specific surface area was measured by nitrogen adsorption at 77 K (BET method) using an automated gas sorption analyzer (Quantachrome Instruments, autosorb – iQ). Zeta potential was measured by the Zetasizer (Nano-ZS) from Malvern Instruments.

2.4. Adsorption experiments

The adsorption experiments were carried out in the shaking table at 200 rpm and 25 ± 1 °C using 150 mL shaking flasks containing different initial concentration of arsenic solutions. The effects of contact time, pH value, adsorption isotherms, coexisting ions

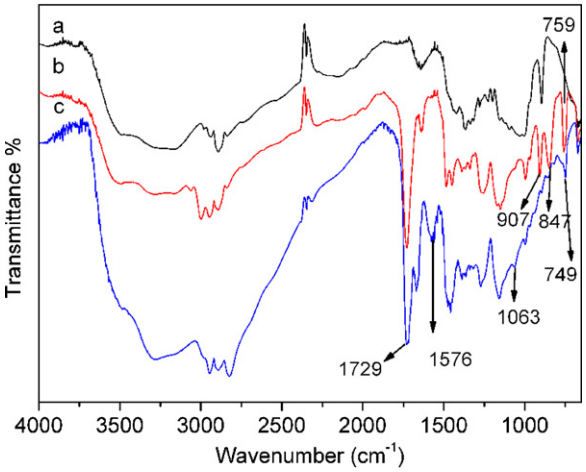

Fig. 1. FTIR spectra of alkali cellulose (a), cellulose-*g*-GMA (b), and cellulose-*g*-GMA-*b*-TEPA (c).

and the regeneration performance on the equilibrium adsorption capacity were investigated. The adsorbent dose was kept as 1 g/L for all the experiments. The pH values of the solution were adjusted by 0.1 mol/L HCl or NaOH. The arsenic concentration in the solution was analyzed using an inductively coupled plasma mission spectroscopy (ICPE-9000, Shimadzu). The adsorption capacity q_e (mg/g) was calculated as described by the following equation:

$$q_e = \frac{(C_0 - C_e)V}{m} \quad (4)$$

where C_0 (mg/L) is the initial arsenic concentration, C_e (mg/L) is the arsenic equilibrium concentration, V (L) is the volume of the aresenic solution and m (g) is the mass of adsorbent.

3. Results and discussion

3.1. Characterization of cellulose-g-GMA and cellulose-g-GMA-b-TEPA

In the present study, according to Eq. (1)–(3), the graft percentage (*G*%) and the epoxy group content (Egc) of cellulose-*g*-GMA was 231.4% and 3.1 mmol/g, respectively, and the mass gain percent (Mgp) of cellulose-*g*-GMA-*b*-TEPA was 31.58%. Supplemental data Table S1 shows the results of elemental analysis of alkali cellulose, cellulose-*g*-GMA and cellulose-*g*-GMA-*b*-TEPA. It is found that there is a little nitrogen (<0.3%) in the alkali cellulose and cellulose-*g*-GMA. However, an obvious increase in relative nitrogen composition (8.84%) after the grafting procedure is observed. The results indicate that the amine-functionalized cellulose is obtained through the amination reaction. Moreover, the nitrogen physicsorption curves are presented in Supplemental data Fig. S1, and the specific surface area of cellulose, cellulose-*g*-GMA and cellulose-*g*-GMA-*b*-TEPA is 1.081, 3.472 and 3.682 m^2/g, respectively.

The FTIR spectra of alkali cellulose, cellulose-*g*-GMA and cellulose-*g*-GMA-*b*-TEPA are presented in Fig. 1. In the spectrum of alkali cellulose (Fig. 1a), the broad band at around 3300 cm^{-1} is attributed to the presence of free and hydrogen bonded OH stretching vibration. The band at 2891 cm^{-1} is due to the C—H stretching vibration and the one at 1429 cm^{-1} corresponds to CH_2 bending vibration. The peak at 1152 cm^{-1} relates to C—O—C antisymmetric stretching vibration. The adsorption band at 1001 cm^{-1} is attributed to C—O stretching vibration. An absorption band at 896 cm^{-1} arises from the β-glycosidic linkages. These peaks are all the characteristic absorption bands of cellulose (Gurgel, de Freitas, & Gil, 2008). After the graft polymerization, a new peak appears

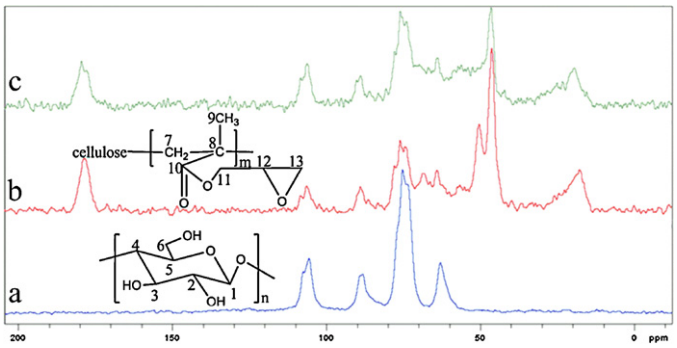

Fig. 2. Solid-state CP/MAS ^{13}C NMR spectra: (a) alkali cellulose; (b) cellulose-*g*-GMA; (c) cellulose-*g*-GMA-*b*-TEPA.

at 1729 cm^{-1} in the cellulose-*g*-GMA (Fig. 1b), which is attributed to the carbonyl group of the ester. The vibration at 1450 cm^{-1} corresponds to the CH_2 scissoring band of PGMA (Wei, Zheng, & Chen, 2011). Three obvious characteristic peaks of epoxy groups appear at 907, 847 and 759 cm^{-1}. All the above results indicate that GMA had been grafted onto the alkali cellulose successfully. Following the amination reaction, three typical characteristic peaks of epoxy groups disappear (Fig. 1c). A broad band in the range of about 3000–3500 cm^{-1} is attributed to the stretching vibration of OH and NH groups. In addition, the new bands appear at 1576, 1063 and 749 cm^{-1}, which can be assigned to the NH deformation vibration, the C—N stretching vibration and the N—H out-of-plane bending vibration in TEPA (Zheng et al., 2011). The above results indicate that TEPA was successfully introduced onto the surface of the cellulose-*g*-GMA.

The NMR spectra of alkali cellulose, cellulose-*g*-GMA and cellulose-*g*-GMA-*b*-TEPA are shown in Fig. 2. In the spectrum of alkali cellulose (Fig. 2a), all signals, i.e. those at 105.5 ppm (C-1), 88.1 ppm (C-4), 75.1 ppm (C-2, C-3 and C-5), and 62.8 ppm (C-6), are attributed to six carbon atoms of the glucose unit, which are characteristic peaks of cellulose (da Silva, de Melo, & Airoldi, 2006). Comparing Fig. 2a–c, there are no changes from 60 ppm to 110 ppm, indicating that the cellulose bulk structure in cellulose-*g*-GMA and cellulose-*g*-GMA-*b*-TEPA is not affected by the polymerization. In the spectrum of cellulose-*g*-GMA (Fig. 2b), some resonances belonging to the PGMA are observed: the methyl resonance (C-9) is at 17.7 ppm; the chemical shift at 46.1 ppm is due to the resonance of the quaternary carbon (C-8) and the methylene carbon (C-13) in the epoxy group; the chemical shift at 50.3 ppm is assigned to the tertiary carbon (C-12) of epoxy group; the carbon resonance (C-10) of carbonyl group appears at 178.5 ppm; the chemical shift at 68.4 ppm and 56.6 ppm corresponds to the methylene resonance of C-7 and C-11, respectively. Furthermore, there is no presence of resonances corresponded to olefinic carbons in the range 120–160 ppm, implying the absence of unreacted GMA (Vismara, Melone, Gastaldi, Cosentino, & Torri, 2009). Comparison of spectra b and c shows that one typical chemical shift for epoxy groups (C-12) disappears after the amination reaction, indicating the successful conversion of the epoxide ring. The opening of the epoxide ring causes a downfield shift of the carbons and gives rise to the CH peak (C-12, 50.3 ppm) being shifted to around 70 ppm (Lamnawar, Baudouin, & Maazouz, 2010). Moreover, the intensity of C-8 and C-13 peaks decreases significantly, and the CH_2 peak of C-13 and TEPA appears at 46.5 ppm (da Silva et al., 2006; Lamnawar et al., 2010). The above results demonstrate that the aminated material is successfully synthesized.

The SEM images of alkali cellulose, cellulose-*g*-GMA and cellulose-*g*-GMA-*b*-TEPA are shown in Fig. 3. It can be observed that the surface morphology of alkali cellulose looks smooth (Fig. 3(a), (d) and (g)). However, after grafting GMA to alkali

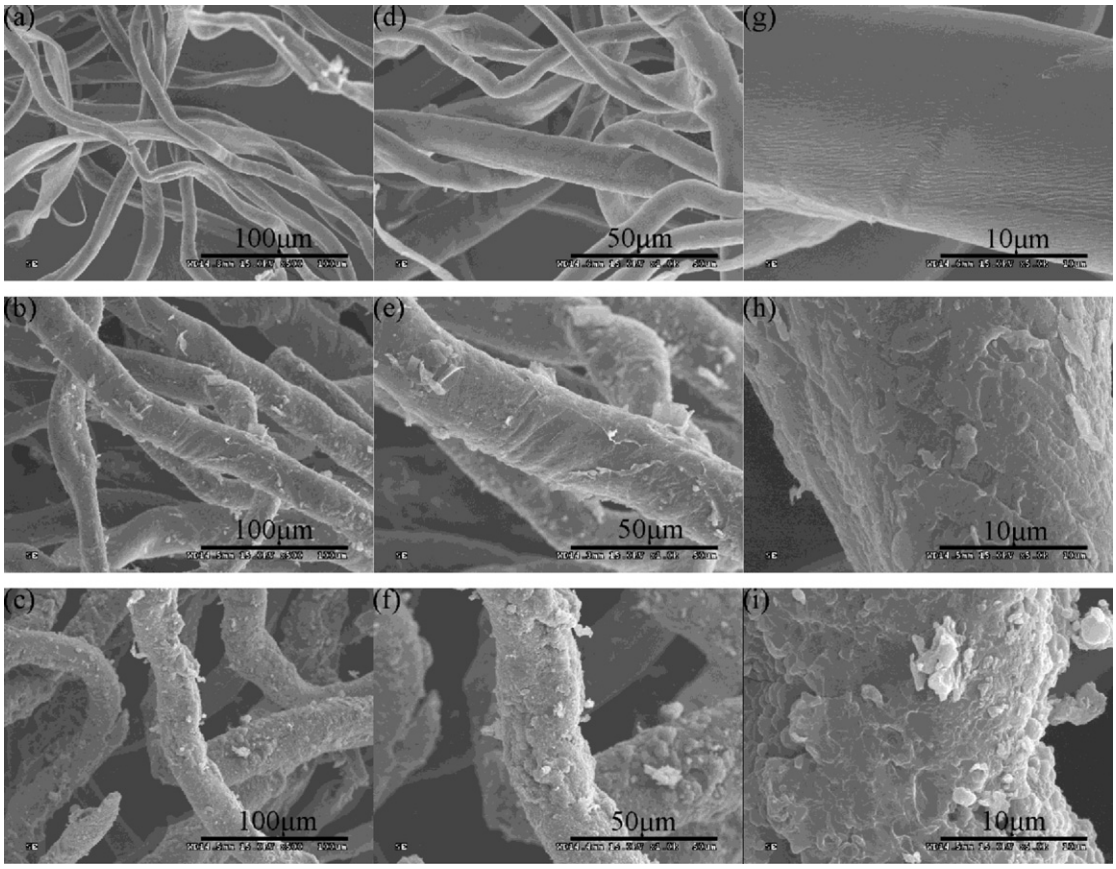

Fig. 3. SEM images of alkali cellulose (a, d and g), cellulose-*g*-GMA (b, e and h) and cellulose-*g*-GMA-*b*-TEPA (c, f and i): (a, b and c) magnification 500×, (d, e and f) magnification 1000×, (g, h and i) magnification 2000×.

cellulose, the surface morphology of cellulose-*g*-GMA is rougher than that of alkali cellulose (Fig. 3(b), (e) and (h)), which is due to the fact that the graft process is a heterogeneous reaction on the surface of alkali cellulose and the grafted GMA chains only cover the surface of cellulose (Zhou et al., 2011). After the amination reaction, numerous obvious coating layers are observed, as shown in Fig. 3(c), (f) and (i). Thus, the results indicate that the amination reaction achieved the immobilization of the TEPA on the surface of cellulose-*g*-GMA.

3.2. Adsorption properties

3.2.1. Kinetic study

The effect of contact time for As(III) and As(V) in aqueous solution is presented in Supplemental data Fig. S2a. It is observed that the adsorption rate was very fast at the initial stage and the adsorption equilibrium was established after 5 min and 300 min for As(III) and As(V), respectively.

In order to clear out the rate of the adsorption process and potential rate-limiting step, the pseudo-first-order kinetic model and the pseudo-second-order kinetic model are used to study the adsorption type and mechanism.

The pseudo-first-order kinetic model is expressed as (Ho, Ng, & McKay, 2000):

$$q_t = q_e(1 - e^{-k_1 t}) \tag{5}$$

where q_t and q_e (mg/g) are the amount of solute at time t (min) and equilibrium, respectively, and k_1 is the rate constant of the pseudo-first-order adsorption (min^{-1}).

The pseudo-second-order kinetic model (Chandra et al., 2010; Ho & McKay, 1999a) is described as:

$$q_t = \frac{k_2 q_e^2 t}{1 + k_2 q_e t} \tag{6}$$

The linearized form of the pseudo-second-order kinetic model can be expressed as:

$$\frac{t}{q_t} = \frac{1}{k_2 q_e^2} + \frac{1}{q_e} t \tag{7}$$

where q_t and q_e (mg/g) are the amount of solute at time t (min) and equilibrium, respectively, and k_2 is the rate constant ($g\,mg^{-1}\,min^{-1}$).

The curves of the pseudo-first-order kinetic model and the pseudo-second-order kinetic model are shown in Supplemental data Fig. S2b and c, and the kinetic parameters are calculated and presented in Supplemental data Table S2. As shown in Table S2, the correlation coefficients of the pseudo-first-order kinetic model were lower, indicating that this model could not explain the adsorption process. This is due to the fact that the pseudo-first-order kinetic model cannot fit well to the whole adsorption process and it is only applicable at the initial stage (Ho & McKay, 1999b). However, the correlation coefficients of the pseudo-second-order kinetic model were higher than that of the pseudo-first-order kinetic model and the values of $q_{e2(theo)}$ are in better agreement with the experimental $q_{e(exp)}$ values than that of $q_{e1(theo)}$. Therefore, it is concluded that the process may be a chemical adsorption process involving valence forces through sharing or exchange of electrons between adsorbent and adsorbate (Bulut & Tez, 2007) and the chemisorptions are the rate-limiting mechanism.

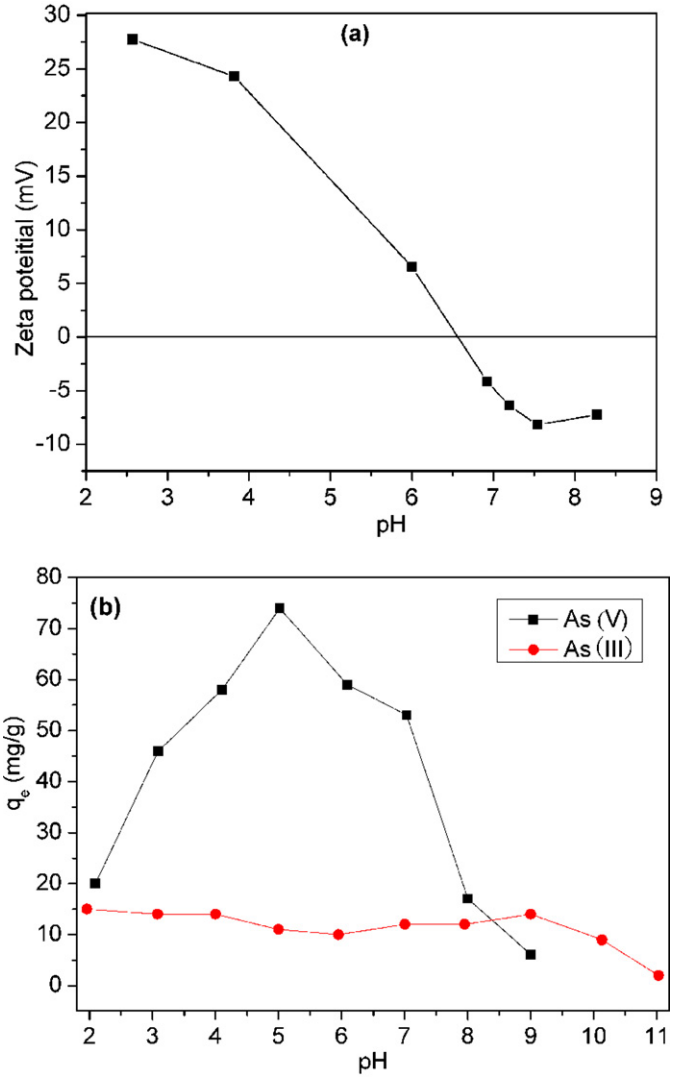

Fig. 4. Zeta potential (a) of cellulose-*g*-GMA-*b*-TEPA and arsenic uptake (b) as a function of pH.

3.2.2. Effect of pH

One important factor in the arsenic removal is the aqueous solution pH, which can affect the adsorbent surface charge and arsenic speciation. Fig. 4 shows zeta potential of cellulose-*g*-GMA-*b*-TEPA and arsenic uptake as a function of pH. As shown in Fig. 4a, the value of zeta potential decreases as pH increases and the point of zero charge (pH_{PZC}) is estimated to be about 6.5. In addition, the adsorption capacity of As(III) in Fig. 4b has no obvious change at $pH \leq 9$ and then decreases with increasing pH. This adsorption behavior is attributed to the different arsenite speciation. At $pH \leq 9$, As(III) is stable as neutral H_3AsO_3, and there are no electrostatic interactions between As(III) species and absorbent surface (Anirudhan, Senan, & Suchithra, 2011). Therefore, the change of adsorbent surface charge does not affect the adsorption of As(III). With the increase of pH, however, the stable species of As(III) are $H_2AsO_3^-$ (pH = 9–12), $HAsO_3^{2-}$ (pH = 12–13), and AsO^{3-} (pH > 13) (Guo & Chen, 2005). Due to this $pH > pH_{PZC}$, the adsorbent surface is negatively charged and there are much electrostatic repulsions between As(III) species and absorbent surface. Therefore, the adsorption capacity decreases with increasing pH. However, it is observed that the effect of pH for As(V) is quite obvious. This is due to the fact that pH affects significantly the speciation of arsenate and the adsorbent surface charge. As the pH increases, the dominant species of arsenate are H_3AsO_4 (pH < 2), $H_2AsO_4^-$ (pH = 2–6.1), $HAsO_4^{2-}$ (pH = 6.1–11.5) and AsO_4^{3-} (pH > 11.5). When the arsenate is absorbed onto the absorbents, the number of consumption adsorption sites for $H_2AsO_4^-$, $HAsO_4^{2-}$, and AsO_4^{3-} is 1, 2 and 3, respectively. Therefore, the maximum adsorption capacity is obtained at pH 5, where the $H_2AsO_4^-$ will predominate in the solution. On the other hand, due to the $pH\ 5 < pH_{PZC}$, the amine groups on the surface of adsorbent can be protonated to form $-NH_3^+$, $-NRH_2^+$ and $-NR_1R_2H^+$, and the adsorbent surface is positively charged. Thus, there are strong electrostatic attractions between As(V) species and absorbent surface. With the increasing of pH, the adsorbent surface charge becomes negative and the dominate species are $HAsO_4^{2-}$, and AsO_4^{3-}. Therefore, the adsorption capacity of As(V) decreases with the increasing of pH.

Table 1
Langmuir, Freundlich and Temkin parameters for As(III) and As(V) adsorption.

	Langmuir parameters		
	Q_{max} (mg/g)	b (L/mg)	R^2
As(III)	5.71	0.21	0.97072
As(V)	75.13	0.079	0.99258
	Freundlich parameters		
	K_f (mg/g)	n	R^2
As(III)	2.11	3.94	0.9261
As(V)	26.85	5.02	0.93441
	Temkin parameters		
	A_T (L/mg)	b_T (J/mol)	R^2
As(III)	4.75	2484.17	0.90697
As(V)	3.36	1791.11	0.92541

3.2.3. Adsorption isotherms

Adsorption isotherms are usually used to describe the relationship between the adsorbent and adsorbate. The most commonly used isotherms are Langmuir, Freundlich and Temkin isotherms. Therefore, in this study, the three isotherms are used to analyze the adsorption experimental data and shown in Supplemental data Fig. S3. The isotherms parameters are calculated and listed in Table 1.

The Langmuir isotherm model is based on the assumption that the adsorbate forms a saturated molecular layer (monolayer) on the adsorbent surface, that the surface sites have the same energy, and that there is no solute-solute or solute-solvent interaction in either phase and transmigration of adsorbate on the plane of the surface (Langmuir, 1918). The Langmuir isotherm model can be expressed as:

$$\frac{Ce}{q_e} = \frac{1}{bQ_{max}} + \frac{Ce}{Q_{max}} \quad (8)$$

where Ce (mg/L) is the equilibrium concentration of arsenic in solution, q_e (mg/g) is the equilibrium adsorption capacity, Q_{max} (mg/g) is the maximum adsorption capacity per gram of sorbent, and b (L/mg) is the Langmuir constant related to the energy of adsorption. In this model, the dimensionless constant separation factor for equilibrium parameter (R_L) (Tian, Wu, Lin, et al., 2011) can be defined as:

$$R_L = \frac{1}{1 + bC_0} \quad (9)$$

where C_0 (mg/L) is the initial concentration of arsenic and b (L/mg) is the Langmuir constant. The value of R_L indicates the type of isotherm to be irreversible ($R_L = 0$), favorable ($0 < R_L < 1$), linear ($R_L = 1$) or unfavorable ($R_L > 1$).

The Freundlich isotherms model (Freundlich, 1906), which assumes a heterogeneous surface and a multilayer adsorption with an energetic nonuniform distribution, can be expressed as:

$$\ln\ q_e = \ln K_f + \frac{1}{n} \ln Ce \tag{10}$$

where Ce (mg/L) is the equilibrium concentration of arsenic in solution, q_e (mg/g) is the equilibrium adsorption capacity, K_f (mg/g) and n are Freundlich constants related to adsorption capacity and heterogeneity factor, respectively.

The Temkin isotherm model considers that due to adsorbent–adsorbate interactions, the heat of adsorption of all the molecules in the layer would decrease linearly with coverage. Therefore, the adsorbent surface is a uniform distribution of binding energies. The Temkin adsorption isotherm expression is shown as:

$$q_e = \frac{RT}{b_T} \ln\ A_T + \frac{RT}{b_T} \ln Ce \tag{11}$$

where Ce (mg/L) is the equilibrium concentration of arsenic in solution, q_e (mg/g) is the equilibrium adsorption capacity, A_T (L/mg) and b_T (J/mol) are the Temkin constants, R (8.314 J/mol K) is the universal gas constant and T is the absolute temperature.

As shown in Table 1, according to the correlation coefficients (R^2), the order of three models which can well fit the experimental data is Langmuir, Freundlich and Temkin. Thus, the Langmuir model is the most suitable to describe the adsorption process of arsenic onto adsorbents and the adsorption is a monolayer adsorption process. The maximum adsorption capacities (Q_{max}) for As(III) and As(V) from Langmuir model are 5.71 mg/g and 75.13 mg/g, respectively. According to Eq. (9), the values of R_L are 0.090–0.373 for As(III) and 0.073–0.158 for As(V), indicating that the adsorption process is favorable. On the other hand, the values of 1/n obtained from Freundlich model are less than 1, which reveals the favorable adsorption of arsenic onto adsorbents. This is consistent with the result of Langmuir model. Temkin model is the worst one in the three models, so it cannot well explain the adsorption process.

The adsorption capacity of cellulose-*g*-GMA-*b*-TEPA for arsenic adsorption from Langmuir isotherm model is compared with that reported by other investigators using other adsorbents. As shown in Table 2, the adsorption of cellulose-*g*-GMA-*b*-TEPA for As(V) is very effective compared with other adsorbents. For As(III) adsorption, the adsorbent cellulose-*g*-GMA-*b*-TEPA presents the moderate adsorption capacity. Thus, the adsorbent cellulose-*g*-GMA-*b*-TEPA has an excellent adsorption ability of arsenic.

3.2.4. Thermodynamics studies

The adsorption process is generally classified by the adsorption heat. In this work, the thermal effect of reversible adsorption process and change in entropy in the course of adsorption are estimated and thermodynamic parameters named Gibbs energy (ΔG), enthalpy change (ΔH) and entropy change (ΔS) are calculated using the following equations (Chen, Lu, Shao, & Luo, 2011):

$$K_D = \frac{(C_0 - C_e)V}{C_e m} \tag{12}$$

$$\ln\ K_D = \frac{\Delta S}{R} - \frac{\Delta H}{RT} \tag{13}$$

$$\Delta G = \Delta H - T\ \Delta S \tag{14}$$

where C_0 and C_e (mg/L) are the initial and equilibrium concentrations of arsenic in solution, respectively, K_D is the distribution coefficient (mL/g), R (8.314 J/mol K) is the universal gas constant, and T is the absolute temperature. The values of ΔH and ΔS were obtained from the slope and intercept of $\ln K_D$ against $1/T$ (Supplemental data Fig. S4). The thermodynamics parameters were listed in Supplemental data Table S3.

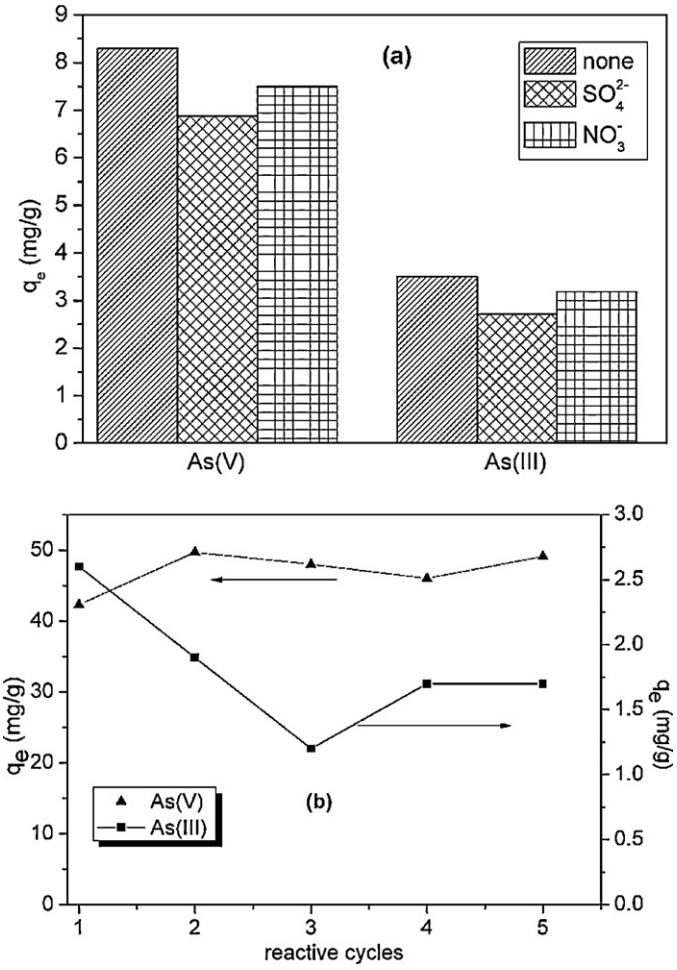

Fig. 5. Effect of coexisting ions (a) and regeneration efficiency (b) onto adsorbent for As(III) (pH = 7) and As(V) (pH = 5).

As shown in Supplemental data Table S3, the negative values of ΔH indicated the exothermic nature of the adsorption process. The negative values of ΔS confirmed a greater order of reaction and the decreased randomness at the solid-solution interface during the adsorption. The positive ΔG for the adsorption of As(III) indicated that the instability activation complex of the adsorption reaction increased with increasing temperature (Negrea et al., 2011). This is in good agreement with the neutral H_3AsO_3 species, which has no electrostatic interactions between As(III) species and absorbent surface. However, the values of ΔG for the adsorption of As(V) were negative, indicating that the adsorption was feasible and spontaneous (Chen et al., 2011).

3.2.5. Effect of coexisting ions

There are various kinds of other anions in the groundwater, such as sulfate and nitrate, which may lead to competitive adsorption. The effects of coexisting ions for arsenic adsorption were studied in the present of 30 mg/L Na_2SO_4 and $NaNO_3$, respectively. Fig. 5a shows the effect of sulfate and nitrate ions on arsenic adsorption. The adsorption capacities of As(III) and As(V) were 8.3 mg/L and 3.5 mg/L, respectively, at initial aresenic concentrations of 10 mg/L without competitive ions. It is noted that the present of sulfate and nitrate has no significant effect on arsenic adsorption. This indicates that sulfate and nitrate binding affinities for active sites is much weaker than arsenic (Guan, Dong, Ma, & Jiang, 2009; Guo and Chen, 2005)

Table 2
Comparison of arsenic adsorption capacity of other adsorbents from Langmuir isotherm model.

Adsorbents	Q_{max} (mg/g)		Reference
	As(III)	As(V)	
Magnetite-graphene hybrids	13.10	5.83	Chandra et al. (2010)
Magnetic wheat straw	3.90	8.06	Tian, Wu, Lin, et al. (2011)
Nano zero-valent@activated carbon	18.19	12.02	Zhu, Jia, Wu, and Wang (2009)
Acidithiobacillus ferrooxidans BY-3	0.293	0.333	Yan et al. (2010)
Fe-coated mesoporous carbon	5.96	5.51	Gu and Deng (2007)
Activated alumina	3.5	15.9	Lin and Wu (2001)
Fe_3O_4 nanomaterial	8.2	6.71	Luther, Borgfeld, Kim, and Parsons (2012)
Fe- amino-GMA-cellulose	–	58.8	Anirudhan et al. (2011)
Cellulose-*g*-GMA-*b*-TEPA	5.71	75.13	This study

3.2.6. Regeneration of adsorbent

In practical application, it is very important to investigate the ability of adsorbent to be regenerated and reused. Regeneration is achieved using 0.1 mol/L NaOH aqueous solution for 1 h. Fig. 5b shows the regeneration efficiency of cellulose-*g*-GMA-*b*-TEPA for As(III) and As(V) with the initial concentration of 50 mg/L and 100 mg/L, respectively. As evident from the results, the adsorption capacity of As(V) does not noticeably change during the four reactive cycles. For As(III), the adsorption capacity of As(III) decreases from 2.6 mg/g to 1.7 mg/g after four reactive cycles. Therefore, the results suggest that the adsorbent has an excellent reusability for the removal of arsenic.

4. Conclusion

A cellulosic adsorbent has been successfully prepared for efficient arsenic removal from the aqueous solution through a two-step surface modification. The elemental analysis, FTIR and ^{13}C NMR characterization demonstrated that the side chain PGMA had been grafted onto the cellulose backbone, and further reacted with TEPA via ring-opening polymerization. SEM images confirmed that the modification occurred on the surface of cellulose. The adsorption process could be explained by the pseudo-second-order kinetic model. The optimal pH for the removal of arsenic was 7 for arsenite and 5 for arsenate, respectively. The Langmuir model could fit the experimental data perfectly and the adsorption capacities were 5.71 mg/g for As(III) and 75.13 mg/g for As(V), respectively. The adsorption behavior was less affected by the coexisting ions and the adsorbent could be reused up to four cycles without much loss of adsorption capacity. Therefore, the cellulosic adsorbent has a great potential to remove arsenic from the aqueous solution.

Acknowledgment

This work was supported by the National Basic Research Program of China (973 Program, No. 2011CB933700) of Ministry of Science and Technology of China.

Appendix A. Supplementary data

Supplementary data associated with this article can be found, in the online version, at http://dx.doi.org/10.1016/j.carbpol.2012.09.050.

References

An, B., Liang, Q. Q., & Zhao, D. Y. (2011). Removal of arsenic(V) from spent ion exchange brine using a new class of starch-bridged magnetite nanoparticles. *Water Research*, *45*(5), 1961–1972.

Anirudhan, T. S., & Senan, P. (2011). Adsorptive potential of sulfonated poly(glycidylmethacrylate)-grafted cellulose for separation of lysozyme from aqueous phase: Mass transfer analysis, kinetic and equilibrium profiles. *Colloids and Surfaces A: Physicochemical and Engineering Aspects*, *377*(1–3), 156–166.

Anirudhan, T. S., Senan, P., & Suchithra, P. S. (2011). Evaluation of iron(III)-coordinated amino-functionalized poly(glycidyl methacrylate)-grafted cellulose for arsenic(V) adsorption from aqueous solutions. *Water Air and Soil Pollution*, *220*(1–4), 101–116.

Anirudhan, T. S., & Unnithan, M. R. (2007). Arsenic(V) removal from aqueous solutions using an anion exchanger derived from coconut coir pith and its recovery. *Chemosphere*, *66*(1), 60–66.

Bulut, Y., & Tez, Z. (2007). Adsorption studies on ground shells of hazelnut and almond. *Journal of Hazardous Materials*, *149*(1), 35–41.

Cao, W., Dang, Z., Zhou, X. Q., Yi, X. Y., Wu, P. X., Zhu, N. W., et al. (2011). Removal of sulphate from aqueous solution using modified rice straw: Preparation, characterization and adsorption performance. *Carbohydrate Polymers*, *85*(3), 571–577.

Chandra, V., Park, J., Chun, Y., Lee, J. W., Hwang, I. C., & Kim, K. S. (2010). Water-dispersible magnetite-reduced graphene oxide composites for arsenic removal. *ACS Nano*, *4*(7), 3979–3986.

Chen, L. H., Lu, L. L., Shao, W. J., & Luo, F. (2011). Kinetics and equilibria of Cd(II) adsorption onto a chemically modified lawny grass with H BTMPP. *Journal of Chemical and Engineering Data*, *56*(4), 1059–1068.

da Silva, E. C., de Melo, J. C. P., & Airoldi, C. (2006). Preparation of ethylenediamine-anchored cellulose and determination of thermochemical data for the interaction between cations and basic centers at the solid/liquid interface. *Carbohydrate Research*, *341*(17), 2842–2850.

Dhoble, R. M., Lunge, S., Bhole, A. G., & Rayalu, S. (2011). Magnetic binary oxide particles (MBOP): A promising adsorbent for removal of As (III) in water. *Water Research*, *45*(16), 4769–4781.

Freundlich, H. (1906). Concerning adsorption in solutions. *Zeitschrift Fur Physikalische Chemie—Stochiometrie Und Verwandtschaftslehre*, *57*(4), 385–470.

Gu, Z. M., & Deng, B. L. (2007). Use of iron-containing mesoporous carbon (IMC) for arsenic removal from drinking water. *Environmental Engineering Science*, *24*(1), 113–121.

Gu, Z. M., Fang, J., & Deng, B. L. (2005). Preparation and evaluation of GAC-based iron-containing adsorbents for arsenic removal. *Environmental Science & Technology*, *39*(10), 3833–3843.

Guan, X., Dong, H., Ma, J., & Jiang, L. (2009). Removal of arsenic from water: Effects of competing anions on As(III) removal in $KMnO_4$–Fe(II) process. *Water Research*, *43*(15), 3891–3899.

Guo, X. J., & Chen, F. H. (2005). Removal of arsenic by bead cellulose loaded with iron oxyhydroxide from groundwater. *Environmental Science & Technology*, *39*(17), 6808–6818.

Gurgel, L. V. A., de Freitas, R. P., & Gil, L. F. (2008). Adsorption of Cu(II), Cd(II), and Pb(II) from aqueous single metal solutions by sugarcane bagasse and mercerized sugarcane bagasse chemically modified with succinic anhydride. *Carbohydrate Polymers*, *74*(4), 922–929.

Gurgel, L. V. A., de Melo, J. C. P., de Lena, J. C., & Gil, L. F. (2009). Adsorption of chromium (VI) ion from aqueous solution by succinylated mercerized cellulose functionalized with quaternary ammonium groups. *Bioresource Technology*, *100*(13), 3214–3220.

Habibi, Y., Lucia, L. A., & Rojas, O. J. (2010). Cellulose nanocrystals: Chemistry, self-assembly, and applications. *Chemical Reviews*, *110*(6), 3479–3500.

Ho, Y. S., & McKay, G. (1999a). Pseudo-second order model for sorption processes. *Process Biochemistry*, *34*(5), 451–465.

Ho, Y. S., & McKay, G. (1999b). The sorption of lead(II) ions on peat. *Water Research*, *33*(2), 578–584.

Ho, Y. S., Ng, J. C. Y., & McKay, G. (2000). Kinetics of pollutant sorption by biosorbents: Review. *Separation and Purification Methods*, *29*(2), 189–232.

Iqbal, J., Kim, H. J., Yang, J. S., Baek, K., & Yang, J. W. (2007). Removal of arsenic from groundwater by micellar-enhanced ultrafiltration (MEUF). *Chemosphere*, *66*(5), 970–976.

Lamnawar, K., Baudouin, A., & Maazouz, A. (2010). Interdiffusion/reaction at the polymer/polymer interface in multilayer systems probed by linear viscoelasticity coupled to FTIR and NMR measurements. *European Polymer Journal*, *46*(7), 1604–1622.

Langmuir, I. (1918). Adsorption of gases on plain surfaces of glass, mica platinum. *Journal of the American Chemical Society*, *40*, 1361–1403.

Lin, T. F., & Wu, J. K. (2001). Adsorption of arsenite and arsenate within activated alumina grains: Equilibrium and kinetics. *Water Research*, *35*(8), 2049–2057.

Luther, S., Borgfeld, N., Kim, J., & Parsons, J. G. (2012). Removal of arsenic from aqueous solution: A study of the effects of pH and interfering ions using iron oxide nanomaterials. *Microchemical Journal*, *101*, 30–36.

Maji, S. K., Pal, A., Pal, T., & Adak, A. (2007). Sorption kinetics of arsenic on laterite soil in aqueous medium. *Journal of Environmental Science and Health Part A: Toxic/Hazardous Substances & Environmental Engineering*, *42*(7), 989–996.

Martin, D. F., O'Donnell, L., Martin, B. B., & Alldredge, R. (2007). Removal of aqueous arsenic using iron attached to immobilized ligands (IMLIGs). *Journal of Environmental Science and Health Part A: Toxic/Hazardous Substances & Environmental Engineering*, *42*(1), 97–102.

Mercer, K. L., & Tobiason, J. E. (2008). Removal of arsenic from high ionic strength solutions: Effects of ionic strength, pH, and preformed versus in situ formed HFO. *Environmental Science & Technology*, *42*(10), 3797–3802.

Moreno-Casillas, H. A., Cocke, D. L., Gomes, J. A. G., Morkovsky, P., Parga, J. R., & Peterson, E. (2007). Electrocoagulation mechanism for COD removal. *Separation and Purification Technology*, *56*(2), 204–211.

Munoz, J. A., Gonzalo, A., & Valiente, M. (2002). Arsenic adsorption by Fe(III)-loaded open-celled cellulose sponge. Thermodynamic and selectivity aspects. *Environmental Science & Technology*, *36*(15), 3405–3411.

Negrea, A., Ciopec, M., Lupa, L., Davidescu, C. M., Popa, A., Ilia, G., et al. (2011). Removal of As(V) by Fe(III)-loaded XAD7 impregnated resin containing di(2-ethylhexyl) phosphoric acid (DEHPA): Equilibrium, kinetic, and thermodynamic modeling studies. *Journal of Chemical and Engineering Data*, *56*(10), 3830–3838.

O'Connell, D. W., Birkinshaw, C., & O'Dwyer, T. F. (2006). A chelating cellulose adsorbent for the removal of Cu(II) from aoueous solutions. *Journal of Applied Polymer Science*, *99*(6), 2888–2897.

O'Connell, D. W., Birkinshaw, C., & O'Dwyer, T. F. (2008). Heavy metal adsorbents prepared from the modification of cellulose: A review. *Bioresource Technology*, *99*(15), 6709–6724.

Roy, D., Semsarilar, M., Guthrie, J. T., & Perrier, S. (2009). Cellulose modification by polymer grafting: A review. *Chemical Society Reviews*, *38*(7), 2046–2064.

Tian, Y., Wu, M., Lin, X. B., Huang, P., & Huang, Y. (2011). Synthesis of magnetic wheat straw for arsenic adsorption. *Journal of Hazardous Materials*, *193*, 10–16.

Tian, Y., Wu, M., Liu, R. G., Wang, D. Q., Lin, X. B., Liu, W. L., et al. (2011). Modified native cellulose fibers—A novel efficient adsorbent for both fluoride and arsenic. *Journal of Hazardous Materials*, *185*(1), 93–100.

Vismara, E., Melone, L., Gastaldi, G., Cosentino, C., & Torri, G. (2009). Surface functionalization of cotton cellulose with glycidyl methacrylate and its application for the adsorption of aromatic pollutants from wastewaters. *Journal of Hazardous Materials*, *170*(2–3), 798–808.

Wei, Y. T., Zheng, Y. M., & Chen, J. P. (2011). Functionalization of regenerated cellulose membrane via surface initiated atom transfer radical polymerization for boron removal from aqueous solution. *Langmuir*, *27*(10), 6018–6025.

Wu, Z. X., Li, W., Webley, P. A., & Zhao, D. Y. (2012). General and controllable synthesis of novel mesoporous magnetic iron oxide@carbon encapsulates for efficient arsenic removal. *Advanced Materials*, *24*(4), 485.

Xu, X., Gao, B. Y., Tan, X., Yue, Q. Y., Zhong, Q. Q., & Li, Q. A. (2011). Characteristics of amine-crosslinked wheat straw and its adsorption mechanisms for phosphate and chromium (VI) removal from aqueous solution. *Carbohydrate Polymers*, *84*(3), 1054–1060.

Xu, X., Gao, B. Y., Yue, Q. Y., Zhong, Q. Q., & Zhan, X. A. (2010). Preparation, characterization of wheat residue based anion exchangers and its utilization for the phosphate removal from aqueous solution. *Carbohydrate Polymers*, *82*(4), 1212–1218.

Yan, L., Yin, H. H., Zhang, S., Leng, F. F., Nan, W. B., & Li, H. Y. (2010). Biosorption of inorganic and organic arsenic from aqueous solution by Acidithiobacillus ferrooxidans BY-3. *Journal of Hazardous Materials*, *178*(1–3), 209–217.

Zhao, Z., Jia, Y., Xu, L., & Zhao, S. (2011). Adsorption and heterogeneous oxidation of As(III) on ferrihydrite. *Water Research*, *45*(19), 6496–6504.

Zheng, Y. Q., Deng, S. B., Niu, L., Xu, F. J., Chai, M. Y., & Yu, G. (2011). Functionalized cotton via surface-initiated atom transfer radical polymerization for enhanced sorption of Cu(II) and Pb(II). *Journal of Hazardous Materials*, *192*(3), 1401–1408.

Zhou, Y. M., Jin, Q. A., Zhu, T. W., & Akama, Y. F. (2011). Adsorption of chromium (VI) from aqueous solutions by cellulose modified with beta-CD and quaternary ammonium groups. *Journal of Hazardous Materials*, *187*(1–3), 303–310.

Zhu, H., Jia, Y., Wu, X., & Wang, H. (2009). Removal of arsenic from water by supported nano zero-valent iron on activated carbon. *Journal of Hazardous Materials*, *172*(2–3), 1591–1596.